EurJIC
European Journal of Inorganic Chemistry

Research Article
doi.org/10.1002/ejic.202200687

Chemistry Europe
European Chemical Societies Publishing

www.eurjic.org

Directed Dehydration of $Na_4Sn_2S_6 \cdot 5H_2O$ Generates the New Compound $Na_4Sn_2S_6$: Crystal Structure and Selected Properties

Assma Benkada[+],[a] Felix Hartmann[+],*[a] Michael Poschmann,[a] Sylvio Indris,[b] Henning Lühmann,[a] and Wolfgang Bensch*[a]

The new thiostannate $Na_4Sn_2S_6$ was prepared by directed crystal water removal from the hydrate $Na_4Sn_2S_6 \cdot 5H_2O$ at moderate temperatures. While the structure of the hydrate comprises isolated $[Sn_2S_6]^{4-}$ anions, that of the anhydrate contains linear chains composed of corner-sharing SnS_4 tetrahedra, a structural motif not known in thiostannate chemistry. This structural rearrangement requires bond-breakage in the $[Sn_2S_6]^{4-}$ anion, movements of the fragments of the opened $[Sn_2S_6]^{4-}$ anion and Sn–S–Sn bond formation. Simultaneously, the coordination environment of the Na^+ cations is significantly altered and the *in situ* formed NaS_5 polyhedra are joined by corner- and edge-sharing to form a six-membered ring. Time-dependent *in situ* X-ray powder diffraction evidences very fast rehydration into $Na_4Sn_2S_6 \cdot 5H_2O$ during storage in air atmosphere, but recovery of the initial crystallinity requires several days. Impedance spectroscopy demonstrates a mediocre room-temperature Na^+ ion conductivity of 0.31 $\mu S\,cm^{-1}$ and an activation energy for ionic transport of $E_a = 0.75$ eV.

Introduction

Several synthetic approaches were established for the preparation of thiostannates and tin sulfides including the high temperature annealing method[1–11] and the so-called molten flux approach.[12–15] In these compounds, the choice of the charge balancing cations is restricted to those, which are stable under the actual conditions, and therefore many compounds contain alkali metal or alkaline earth metal cations. Another widely applied method is the solvothermal approach, which has the important advantage that complexes or organic cations can be integrated into the thiometallate networks besides simple metal cations. Furthermore, the structural diversity and dimensionality is much larger than for thiometallates obtained by the synthetic routes mentioned above and feature molecules, chains, layers and networks.[16–22] There are also some reports that thiostannates can be prepared under even milder reaction conditions in liquid media.[23–27] Several thiostannates or tin sulfides exhibit interesting and promising properties like non-linear optical behavior,[28] the selective capture of hazardous or radioactive metal cations,[29–31] as absorber layers in thin film solar cells,[32–34] as photocatalyst for light-driven hydrogen evolution,[35] or as luminescent material.[36] In the last few years, tin-based sulfides came into focus of research in the area of energy storage materials[37] as well as solid electrolytes for applications in all-solid-state batteries, because some exhibit superionic conduction properties. For example, the mixed quaternary compounds $Na_{11}Sn_2PS_{12}$ ($\sigma_{RT} = 3.7$ mS cm^{-1} and $E_a = 0.39$ eV; $\sigma_{RT} = 1.4$ mS cm^{-1} and $E_a = 0.25$ eV),[38,39] $Na_{10}SnP_2S_{12}$ ($\sigma_{RT} = 0.4$ mS cm^{-1}, $E_a = 0.36$ eV),[40] $Na_{11}Sn_2SbS_{12}$ ($\sigma_{RT} = 0.6$ mS cm^{-1}, $E_a = 0.34$ eV),[41] $Na_{11.25}Sn_{2.25}Sb_{0.75}S_{12}$ ($\sigma_{RT} = 0.5$ mS cm^{-1}, $E_a = 0.39$ eV)[42] have promisingly high room-temperature (RT) conductivities σ_{RT} and low activation energies E_a for ionic conduction. In contrast, ternary sodium thiostannates such as the two polymorphs of Na_4SnS_4 ($\sigma_{RT} = 2.2 \times 10^{-3}$ mS cm^{-1} and $E_a = 0.51$ eV; $\sigma_{RT} = 1 \times 10^{-5}$ mS cm^{-1}, $E_a = 0.65$ eV)[43] or sodium selenostannates such as Na_4SnSe_4 ($\sigma_{RT} = 2.2 \times 10^{-5}$ mS cm^{-1}, $E_a = 0.28$ eV)[44] exhibit significantly worse ionic conduction properties compared to ternary sodium thiophosphates and thioantimonates like Na_3PS_4 ($\sigma_{RT} = 0.2$ mS cm^{-1}, $E_a = 0.35$ eV)[45] and Na_3SbS_4 ($\sigma_{RT} = 3.0$ mS cm^{-1}, $E_a = 0.25$ eV).[46]

Most of the aforementioned potential solid electrolytes were synthesized at elevated temperatures and required elaborate preparation procedures. An elegant but not often applied synthetic approach is the directed thermal removal of crystal water molecules or labile ligands as demonstrated for Li chalcogenidostannates,[47,48] Na_3SbS_4,[49] and $Na_{4-x}Sn_{1-x}Sb_xS_4$.[43] In the latter study, we have shown that a new metastable polymorph of Na_4SnS_4 can be obtained by this approach starting from $Na_4SnS_4 \cdot 14H_2O$.[43] Another possible suitable candidate for such a synthetic procedure is $Na_4Sn_2S_6 \cdot 5H_2O$ (**I**)

[a] Dr. A. Benkada,[+] F. Hartmann,[+] Dr. M. Poschmann, H. Lühmann, Prof. Dr. W. Bensch
Christian-Albrecht University of Kiel, Institute of Inorganic Chemistry
Max-Eyth-Straße 2, 24118 Kiel (Germany)
E-mail: fhartmann@ac.uni-kiel.de
wbensch@ac.uni-kiel.de
https://www.ac.uni-kiel.de/de/bensch/startseite

[b] Dr. S. Indris
Karlsruhe Institute of Technology, Institute of Applied Materials
Hermann-von-Helmholtz-Platz 1,
76344 Eggenstein-Leopoldshafen (Germany)

[+] These authors contributed equally to this work.

Supporting information for this article is available on the WWW under https://doi.org/10.1002/ejic.202200687

Research Article
doi.org/10.1002/ejic.202200687

which can be easily prepared under moderate conditions in good yields. Here we report the synthesis of the new compound $Na_4Sn_2S_6$ (**II**), the crystal structure, ^{119}Sn and ^{23}Na Magic-angle spinning (MAS) NMR and Raman spectra, and the results of electrochemical impedance spectroscopy (EIS) investigations.

Results and Discussion

The thermal stability of $Na_4Sn_2S_6 \cdot 5H_2O$ (**I**) was investigated and the TG curve ($T_{final} = 300\,°C$, heating rate: 4 K min^{-1}) shows two not well-resolved mass steps (Figure 1), which are accompanied by endothermic events in the DTA curve ($T_p = 95$ and 132 °C). The experimental mass loss of 16.7 % is finished at $T \approx 150\,°C$ and slightly larger than that calculated for the removal of all crystal water molecules (calc.: 14.7 %). Applying a lower heating rate of 1 K min^{-1} (Figure S1) leads to a similar mass change (16.9 %) in almost one step with an endothermic signal at $T_p = 128\,°C$. In both thermal decomposition reactions, the new dehydrated compound $Na_4Sn_2S_6$ (**II**) was formed as identified by crystal structure determination from powder X-ray diffraction (PXRD) data (see below).

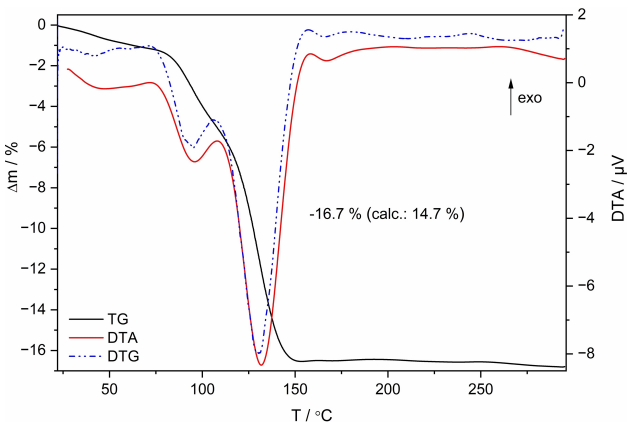

Figure 1. TG (black), DTA (red) and DTG (dashed-dotted blue) of $Na_4Sn_2S_6 \cdot 5H_2O$ (**I**) performed with a heating rate of 4 K min^{-1} in N_2 atmosphere.

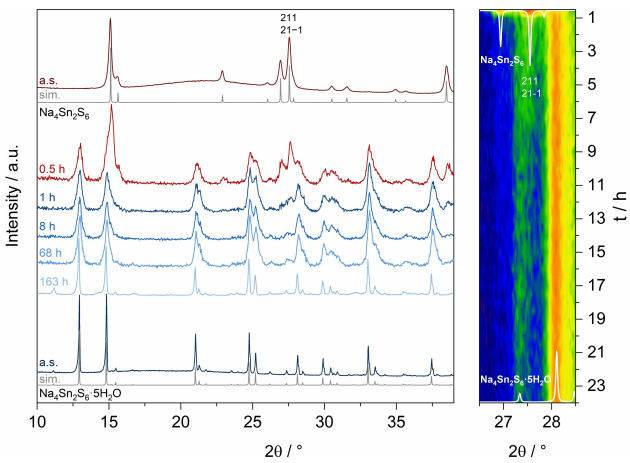

Figure 2. Selected patterns (left) and logarithmic intensity contour profile between 26.5° and 28.5° 2θ (right) of a time-dependent PXRD experiment during rehydration of $Na_4Sn_2S_6 \cdot 5H_2O$ (**I**) into $Na_4Sn_2S_6$ (**II**) during storage at 295 K in air atmosphere. A comparison with simulated (sim.) and experimental PXRD of as synthesized (a.s.) **I** and **II** is shown as well.

To examine whether compound **II** absorbs water from atmosphere it was stored in air ($T = 295$ K, room humidity 30-45 %) and time-dependent PXRD patterns were collected every 30 min (Figures S2–S4); selected patterns are shown in Figure 2 (left). In the very first scan of this experiment ($t = 0$ to 0.5 h), reflections corresponding to **I** and **II** are observed. After 1 h, the rehydration of **II** into **I** seems to be almost finished and the starting compound **I** is recovered as a slightly yellow solid. However, a closer look at the intensity evolution of, for example, the 211/21-1 reflection of **II** during the first 24 h of the time-dependent *in situ* experiment (Figure 2, right) reveals that a part of the dehydrated thiostannate survives for ≈8 h. However, after 8 h, the hydrated thiostannate **I** is fully recovered and during the next 60 h, no significant alterations can be observed *via* PXRD. After several days storage in air atmosphere ($t_{total} = 163$ h), another PXRD was collected and the reflections became sharper compared to the PXRD obtained after 68 h, thus the coherently scattering domains of **I** grew during the storage process leading to an improved crystallinity. The results demonstrate that the crystal water molecules of **I** can be reversibly removed with good crystallinity after incorporation of H_2O in the dehydrated material. Since the space group ($P4_12_12$)[50] of the pristine hydrate is enantiomorphic, the chirality of the rehydrated product could differ from the initial one, which needs to be addressed in comprehensive studies in future research. Nonetheless, small fractions of an unknown side phase are detected after storage for 163 h, which are not observed after air exposure of **II** for 68 h (see Figure S4). This may indicate a long-term instability of **I** in air atmosphere.

The new compound $Na_4Sn_2S_6$ (**II**) crystallizes in the non-centrosymmetric orthorhombic space group *Ama*2, with lattice parameters $a = 7.76145(9)$, $b = 11.33324(14)$, $c = 6.83986(9)$ Å, $V = 601.65(1)$ Å^3 and $Z = 2$ as confirmed by Rietveld refinement of the PXRD pattern (Figure 3). In the structure (Figure 4) one unique Na^+ cation is in a general position (8*c*), while three independent S^{2-} anions (4*a*, 4*b*, and 4*b*) and one unique Sn^{4+} cation (4*b*) are in special positions. The Sn^{4+} cation is in a tetrahedral environment with Sn–S bond lengths varying from 2.333(2) to 2.503(2) Å (average: 2.424 Å). The S–Sn–S angles are from 101.67 to 115.36° indicating a severe distortion of the tetrahedron, but the values agree with literature data.[16–27] The structure contains linear $\{Sn_2S_6\}_n$ chains along [010] formed by corner-sharing of SnS_4 units (Figure 4, bottom left). To the best of our knowledge, similar nearly linear chains were not reported in crystal structures of thiostannates. Using the nomenclature developed for silicate structures,[51] the chain represents an unbranched 'einer' single chain (anion periodicity $P = 1$) and the structural formula can be denoted as $Na_4^{[5]}\{uB,\ 1^1_\infty\}[SnS_3]_2$. In contrast to this unique feature in the structure of the title compound, the lowest periodicity of unbranched silicates is $P = 2$ ('zweier' single chain), hence with apexes of neighbored SiO_4

Research Article
doi.org/10.1002/ejic.202200687

Chemistry Europe
European Chemical Societies Publishing

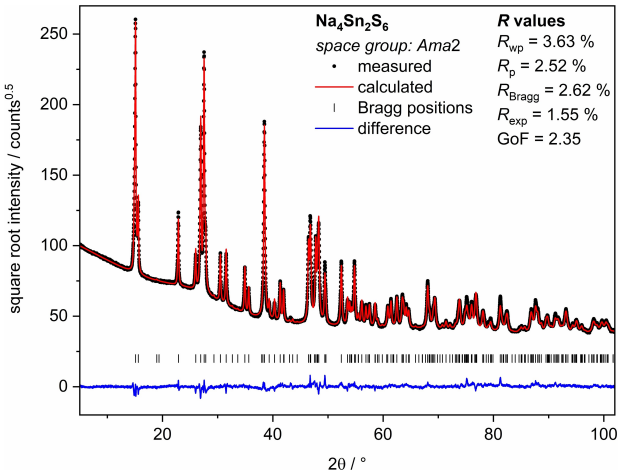

Figure 3. Rietveld plot of the refined crystal structure of $Na_4Sn_2S_6$ (**II**).

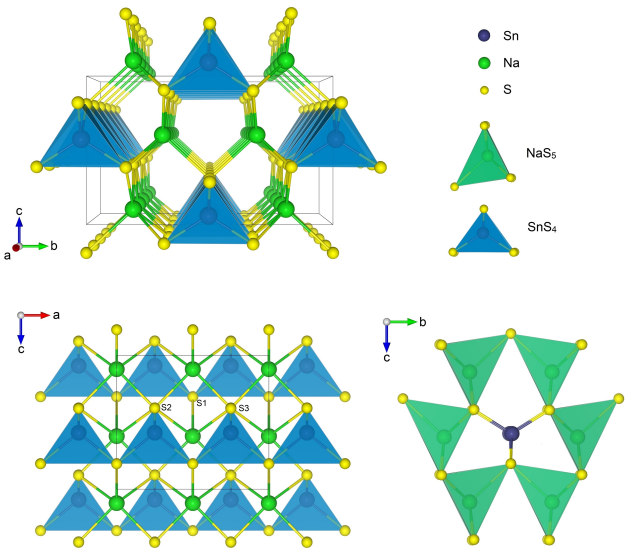

Figure 4. Crystal structure of compound **II**: Perspective view of the 3D network along [100] (top) and parallel view along [010] (bottom left), showcasing the $\{Sn_2S_6\}_n$ chains (blue). Selected atoms are labeled. The interconnection of the NaS_5 polyhedra (green) forms tunnels along [100] (bottom right), which center the $\{Sn_2S_6\}_n$ chains.

tetrahedra in the chain pointing alternately up and down. The unique Na^+ cation is in a fivefold, distorted square pyramidal coordination and these NaS_5 polyhedra are interconnected by edge- and corner-sharing to form a six-membered ring. Along [001] the rings are condensed by edge-sharing of adjacent NaS_5 pyramids and this connection mode generates tunnels directed along [100] (Figure 4, bottom right) which host the Sn atoms. The SnS_4 tetrahedron is surrounded by twelve Na^+ cations *via* Sn–S–Na bonds with Na–S bond lengths ranging from 2.776 to 2.956 Å. The longest bonds are slightly larger than the sum of the ionic radii of 2.84 Å (r_{Na}(CN = 5): 1.00 Å, S^{2-}: 1.84 Å; Sn^{4+}: 0.55 Å).[52] The next nearest S^{2-} anion is located at 3.775 Å, which is far too long for a significant Na···S interaction. All S^{2-} anions have bonds to Na^+ cations: S1 to two, S2 and S3 to four Na^+ cations (Figure S5). Including the S–Sn bonds S1 is in a tetrahedral SNa_2Sn_2 environment, while S2/S3 are in a distorted SNa_4Sn coordination geometry with Sn located at the apex of the distorted square pyramidal polyhedron. The S2 and S3 centered polyhedra share a common edge to form a $S_2Na_6Sn_2$ moiety as secondary building unit, which is bound to two S1 centered polyhedra *via* μ_3-acting Na atoms.

The structure of the pristine compound **I** (space group: $P4_12_12$) was previously described elsewhere with $a = b = 8.45088(3)$ and $c = 23.32912(12)$ Å, $V = 1666.102$ Å^3 and contains isolated edge-sharing double-tetrahedra $[Sn_2S_6]^{4-}$ (Figure S6).[50] The mechanism of the structural transformation of these double-tetrahedra into corner-sharing SnS_4 tetrahedra observed in the chains of **II** is not clear. But notably, **I** and **II** apparently exhibit a topotaxial relationship (cf. Figure S7) with lattice parameters being $a(\mathbf{II}) \approx 1/3 \times c(\mathbf{I})$, $b(\mathbf{II}) \approx 4/3 \times b(\mathbf{I})$, and $c(\mathbf{II}) \approx 4/5 \times a(\mathbf{I})$. One may speculate that during the transformation one of the Sn-S_{bridge}-Sn bonds is opened and adjacent polyhedra are joined by a common S^{2-} anion. From a mechanistic point of view, Sn–S bond breakage in the $[Sn_2S_6]^{4-}$ anion results in two scenarios: i) only one of the Sn–S–Sn bridges is opened leaving behind two different fragments (formally $SnS_{3.5}$ and $SnS_{2.5}$) which are still joined by one S^{2-} anion; ii) both Sn–S–Sn bridges are opened and two SnS_3 moieties are formed. Option i) seems to be unlikely and scenario ii) is more probable. For generation of a linear chain the SnS_3 fragments must slightly rotate and move some Å before Sn–S bond formation can be realized. In addition, a pronounced restructuring occurs around the Na^+ cations involving Na–O bond breakage, Na–S bond formation and some movement of the cations.

The $[Sn_2S_6]^{4-}$ anion has the D_{2h} symmetry and a vibrational analysis yields Equation (1).[50]

$$\Gamma_{vib}^{D2h} = 4\ A_g(Ra) + 2\ B_{1g}(Ra) + 2\ B_{2g}(Ra) + 1\ B_{3g}(Ra) + 1\ A_u(inactive) + 3\ B_{1u}(IR) + 2\ B_{2u}(IR) + 3\ B_{3u}(IR) \quad (1)$$

If the symmetry is reduced to C_i due to the interactions with the Na^+ cations vibrations according to Equation (2) can be expected.[50]

$$\Gamma_{vib}^{Ci} = 9\ A_g(Ra) + 9\ A_u(IR) \quad (2)$$

In the Raman spectrum, the typical Sn–S modes of the $[Sn_2S_6]^{4-}$ anion are observed between 450 and 50 cm^{-1} (Figure 5). The Sn-S_{term} resonance occurs at 377 cm^{-1}, while the Sn–S–Sn bands are observed at 342 (υ_{as}) and at 304 cm^{-1} (υ_s). The Sn_2S_2 ring vibration is located at 284 cm^{-1}. The deformation and lattice vibrations are between 200 and 50 cm^{-1}, but no reasonable assignment can be performed in this region.

MAS NMR spectroscopy was performed to gain deeper insight into the atomic environments of ^{119}Sn and ^{23}Na in the new compound $Na_4Sn_2S_6$ and the results are shown in Figure 6 (for full spectral range see Figure S8). Besides rotational side bands, only a single isotropic peak at 63.6 ppm is observed in the ^{119}Sn MAS NMR spectrum (Figure 6a) representing Sn^{4+}

Research Article
doi.org/10.1002/ejic.202200687

Chemistry Europe
European Chemical Societies Publishing

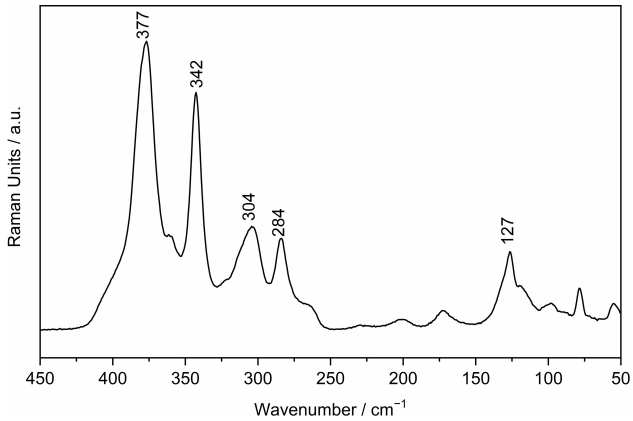

Figure 5. Raman spectrum for $Na_4Sn_2S_6$ (**II**).

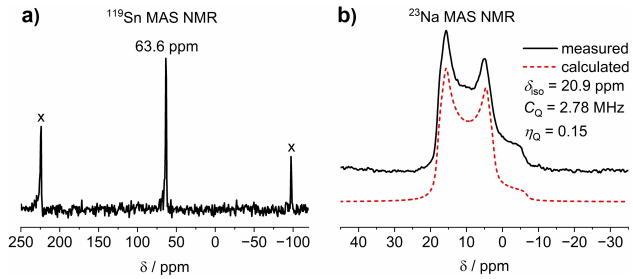

Figure 6. Experimental a) ^{119}Sn and b) ^{23}Na MAS NMR and calculated spectrum for $Na_4Sn_2S_6$ (**II**). Rotational sidebands are marked with crosses.

cations in tetrahedral coordination by S^{2-} and being in line with the observation of solely one independent crystallographic site for Sn by PXRD. The chemical shift is similar to values reported for SnS_4 tetrahedra in the solid compounds Na_4SnS_4,[53] $Na_6Sn_2S_7$,[54] and for $[SnS_4]^{4-}$ units in the liquid state.[35,54] In the ^{23}Na MAS NMR spectrum (Figure 6b), again a single contribution is visible. This contribution has a quadrupolar line shape characterized by an isotropic shift $\delta_{iso} = 20.9$ ppm, quadrupolar coupling constant $C_Q = 2.78$ MHz, and anisotropy parameter $\eta_Q = 0.15$. The spectrum reveals that only a single crystallographic Na site is present in the crystal structure with asymmetric environment around this site, consistent with the distorted square pyramidal S^{2-} coordination detected by XRD. Both the narrow line shape observed for ^{119}Sn (nuclear spin $I = 1/2$) and the clear quadrupolar line shape observed for ^{23}Na ($I = 3/2$) hint at a high crystallinity of this sample.

The Na^+ cation motion properties of $Na_4Sn_2S_6$ were investigated by electrochemical impedance spectroscopy (EIS) between 0 to 70 °C. A representative Nyquist plot recorded at RT is shown in Figure 7 (spectra at different temperatures see Figure S9). All AC impedance spectra were fitted with an equivalent circuit as shown in Figure 7: one resistor (R) in parallel with a constant phase element (CPE) represents the averaged bulk and grain boundary (GB) resistance (single depressed semicircle) and another CPE in series contributes for the blocking electrode behavior (sloping line) at small

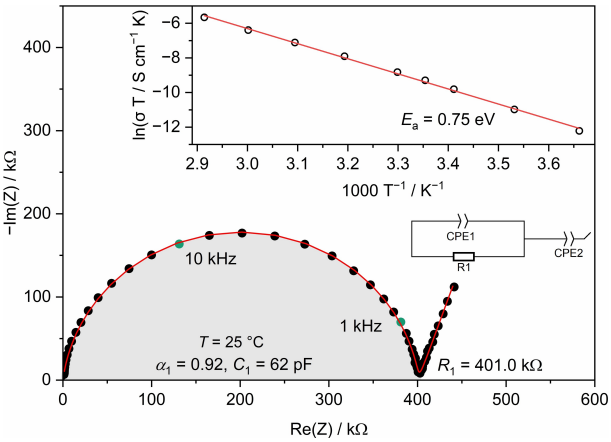

Figure 7. Nyquist plot recorded at 25 °C for $Na_4Sn_2S_6$ (**II**) and equivalent circuit; AC impedance spectra for the Arrhenius plot (top, inset) was recorded from 0 to 70 °C (cf. Table 1).

frequencies.[43,45,55] The Na^+ cation conductivities σ and capacitances C at different temperatures are summarized in Table 1. Values for C correspond to averaged bulk and GB transport behavior if compared to empirical characteristics reported in Ref. [56] ($C_{bulk} \approx 1$ pF, $C_{GB} \approx 4$ nF). The EIS experiments demonstrate decent Na^+ cation motion properties with σ covering several orders of magnitude between 0 and 70 °C. For example, $\sigma_{RT} = 3.1 \times 10^{-4}$ mS cm^{-1} is found for $Na_4Sn_2S_6$, which is comparable to values reported for Na_4SnS_4 or Na_4SnSe_4 (see introduction). Using the temperature-dependent data, E_a was calculated by Equation (3):

$$\sigma \times T = A \times \exp[-E_a/(k_B \times T)] \quad (3)$$

Here, A is the pre-exponential factor, k_B the Boltzmann constant, and T the absolute temperature. σ of $Na_4Sn_2S_6$ follows the Arrhenius law (Figure 7, inset) in the whole temperature regime and a large $E_a = 0.75$ eV indicates that the Na^+ cation motion is highly temperature-driven in this new thiostannate.

Table 1. Ionic conductivities σ and capacitances C_i recorded at various temperatures for $Na_4Sn_2S_6$ (**II**).

T/°C	σ/μS cm^{-1}	C_i/pF
0	0.02	65
10	0.06	57
20	0.19	56
25	0.31	62
30	0.49	62
40	1.17	60
50	2.52	59
60	5.01	60
70	10.2	53

Research Article
doi.org/10.1002/ejic.202200687

Conclusion

We demonstrated that the directed thermal removal of crystal water molecules from $Na_4Sn_2S_6 \cdot 5H_2O$ yields the new compound $Na_4Sn_2S_6$. The removal of H_2O is accompanied by large structural rearrangements and the $[Sn_2S_6]^{4-}$ anion is transformed into a linear $\{Sn_2S_6\}_n^{4n-}$ chain anion which is composed of corner-sharing SnS_4 tetrahedra, a structural feature never reported before in thiostannate chemistry. In the crystal water containing thiostannate the Na^+ cations are in an octahedral (NaO_3S_3) and a trigonal-bipyramidal (NaO_2S_3) geometry, while in $Na_4Sn_2S_6$ the Na^+ cation is in a distorted rectangular-pyramidal (NaS_5) environment, which again requires pronounced structural changes. Nevertheless, the crystallinity of the dehydrated samples was good enough for a structure solution and structure refinement from PXRD. The ^{119}Sn and ^{23}Na MAS NMR spectra show only one signal in accordance with the presence of only one unique Sn and one independent Na atom in the crystal structure. EIS results demonstrate moderate Na^+ ion conductivity for $Na_4Sn_2S_6$ comparable to values previously reported for different ternary sodium thiostannates such as Na_4SnS_4. The presented synthesis route and results now encourage further research to tailor the sodium conduction properties of the new thiostannate by chemical engineering, for example, by cation and anion doping.

Experimental Section

Synthesis of $Na_4Sn_2S_6 \cdot 5H_2O$ (I): 0.750 g (1.27 mmol) $Na_4SnS_4 \cdot 14H_2O$ was dispersed in 4 mL MeOH and heated for 20 min at 90 °C. The white solid of $Na_4Sn_2S_6 \cdot 5H_2O$ was filtrated, washed with MeOH and dried in air at room temperature (yield ≈ 40 % based on Sn).

Synthesis of $Na_4Sn_2S_6$ (II): About 1.0 g (1.6 mmol) $Na_4Sn_2S_6 \cdot 5H_2O$ was placed in an inert gas tube furnace, flushed with dry N_2 gas for 5 min and then heated at a rate of 4 K min^{-1} and N_2 gas flow of about 1 L min^{-1}. At a temperature of 300 °C, the product was quenched to RT in Ar atmosphere and directly transferred into an Ar-filled glovebox without contact to air atmosphere.

Powder X-Ray Diffraction (PXRD): The PXRD patterns were measured with a STOE Stadi-P diffractometer equipped with a MYTHEN 1 K detector (DECTRIS) in transmission geometry using monochromatized Cu–Kα_1 radiation ($\lambda = 1.540598$ Å). For that, compound **II** was loaded into a glass capillary (Hilgenberg, Germany), which was sealed with beeswax. The *in situ* (time-dependent) PXRD experiment was performed in Bragg-Brentanto geometry on a PANalytical Empyrean diffractometer equipped with a PIXcel 1D detector using Cu–Kα radiation and a zero-background sample holder. The sample holder was filled with compound **II** in an Ar-filled glovebox, then transferred to the diffractometer in inert gas atmosphere, finally exposed to air atmosphere the moment the first measurement started and PXRD patterns were collected within 30 min each for 68 h.

Structure Determination: The PXRD pattern of **II** could be indexed using TOPAS Academics[57] yielding three different space groups with comparable quality criteria: the non-centrosymmetric monoclinic space group *C*2 and the non-centrosymmetric orthorhombic space groups *Amm*2 and *Ama*2. The positions of the heavy atoms Sn, S and Na atoms could be determined using direct methods as implemented in Expo 2009.[58] The initial structure models were refined by the Rietveld method in all three cases using a Thompson-Cox-Hastings profile function and a 12th order polynomial background function. Residual electron density was identified by Fourier synthesis and attributed to oxygen atoms representing water molecules coordinated to the sodium atoms. The positions of all atoms were freely refined without any restrains. The isotropic displacement factors were refined element specifically. At the end of the refinements the results were checked with the ADDSYM subroutine implemented in the PLATON software suite. According to the check the most probable space group is *Ama*2 and therefore we decided to report the structural and crystallographic data in this space group. CSD-2208659 (**II**)[59] contains the supplementary crystallographic data for this paper.

Deposition Number(s) 2208659 (**II**) contain(s) the supplementary crystallographic data for this paper. These data are provided free of charge by the joint Cambridge Crystallographic Data Centre and Fachinformationszentrum Karlsruhe Access Structures service.

Thermogravimetry (TG) and Differential Thermal Analysis (DTA): TG and DTA were performed using a Linseis STA PT1600 instrument. The samples were heated in a nitrogen atmosphere with a heating rate of 1 and 4 K min^{-1}, respectively.

Magic-angle spinning (MAS) nuclear magnetic resonance (NMR) spectroscopy: ^{23}Na and ^{119}Sn MAS NMR spectroscopy was performed with a Bruker Avance 500 MHz spectrometer at a magnetic field of 11.7 T, corresponding to resonance frequencies of 132.3 and 186.5 MHz, respectively. Spinning was performed in 2.5 mm rotors at 30 kHz. ^{23}Na NMR spectra were acquired with a Hahn-echo pulse sequence, a $\pi/2$ pulse length of 2.65 µs, and a recycle delay of 30 s. ^{119}Sn NMR spectra were measured with a one-pulse sequence, a $\pi/2$ pulse length of 1.2 µs, and a recycle delay of 30 s. ^{23}Na NMR spectra were referenced to an aqueous 1 m NaCl solution at 0 ppm and ^{119}Sn NMR spectra were referenced to well crystalline SnO_2 at −604.3 ppm.[60]

Electrochemical impedance spectroscopy (EIS): EIS was performed using a VSP Essential (Bioogic) and a test cell for solids ASC–A (Sphere™) with stainless steel pistons as blocking electrodes. Powder of $Na_4Sn_2S_6$ was pressed into pellets ($d = 8.0$ mm, $h = 0.62$ mm) at RT and applying a pressure of $p \approx 120$ MPa. The cell was heated to 70 °C in a climate chamber MK056 (Binder) and tested at various temperature steps during cooling to 0 °C. At each temperature, three alternating current (AC) impedance spectra were recorded with an amplitude of 100 mV in a frequency range from 1 MHz to 1 Hz after temperature acclimatization for 3.5 h. The ionic conductivities were determined as average for each temperature applying fits according to the equivalent circuit shown in Figure 7 using EC-Lab® v11.33.

Supporting Information

The Supporting Information provides further PXRD patterns, MAS NMR and EIS spectra, TG-DTA results as well as additional information about the crystal structures of **I** and **II**.

Acknowledgements

Financial support by the State of Schleswig-Holstein is gratefully acknowledged. We thank Aleksej Jochim, Carsten Wellm, and Inke

Jeß for the TG measurements. Open Access funding enabled and organized by Projekt DEAL.

Conflict of Interest

The authors declare no conflict of interests.

Data Availability Statement

The data that support the findings of this study are available from the corresponding author upon reasonable request.

Keywords: Crystal structure · Impedance spectroscopy · NMR spectroscopy · Sodium thiostannate · Solid-phase synthesis

[1] B. Krebs, W. Schiwy, *Z. Anorg. Allg. Chem.* **1973**, *398*, 63–71.
[2] C. L. Teske, *Z. Anorg. Allg. Chem.* **1978**, *445*, 193–201.
[3] A. Kumari, K. Vidyasagar, *J. Solid State Chem.* **2007**, *180*, 2013–2019.
[4] J.-C. Jumas, E. Philippot, F. Vermot-Gaud-Daniel, M. Ribes, M. Maurin, *J. Solid State Chem.* **1975**, *14*, 319–327.
[5] K. Feng, X. Zhang, W. Yin, Y. Shi, J. Yao, Y. Wu, *Inorg. Chem.* **2014**, *53*, 2248–2253.
[6] L. D. Gulay, I. P. Ruda, O. V. Marchuk, I. D. Olekseyuk, *J. Alloys Compd.* **2008**, *457*, 204–208.
[7] J. A. Aitken, J. W. Lekse, J.-L. Yao, R. Quinones, *J. Solid State Chem.* **2009**, *182*, 141–146.
[8] J. W. Lekse, B. M. Leverett, C. H. Lake, J. A. Aitken, *J. Solid State Chem.* **2008**, *181*, 3217–3222.
[9] R. Pocha, M. Tampier, R.-D. Hoffmann, B. D. Mosel, R. Pöttgen, D. Johrendt, *Z. Anorg. Allg. Chem.* **2003**, *629*, 1379–1384.
[10] K. O. Klepp, *Z. Naturforsch. B* **1992**, *47*, 197–200.
[11] G. Eulenberger, *Z. Naturforsch. B* **1981**, *36*, 687–690.
[12] J. H. Liao, C. Varotsis, M. G. Kanatzidis, *Inorg. Chem.* **1993**, *32*, 2453–2462.
[13] G. A. Marking, M. Evain, V. Petricek, M. G. Kanatzidis, *J. Solid State Chem.* **1998**, *141*, 17–28.
[14] M. G. Kanatzidis, A. C. Sutorik, *Prog. Inorg. Chem.* **1995**, *43*, 151–265.
[15] M. S. Devi, K. Vidyasagar, *J. Chem. Soc. Dalton Trans.* **2002**, 2092–2096.
[16] W. S. Sheldrick, *J. Chem. Soc. Dalton Trans.* **2000**, 3041–3052.
[17] W. S. Sheldrick, M. Wachhold, *Coord. Chem. Rev.* **1998**, *176*, 211–322.
[18] S. Dehnen, M. Melullis, *Coord. Chem. Rev.* **2007**, *251*, 1259–1280.
[19] B. Seidlhofer, N. Pienack, W. Bensch, *Z. Naturforsch. B* **2010**, *65, 937–975*.
[20] Q.-Y. Zhu, J. Dai, *Coord. Chem. Rev.* **2017**, *330*, 95–109.
[21] K.-Y. Wang, M.-L. Feng, X.-Y. Huang, J. Li, *Coord. Chem. Rev.* **2016**, *322*, 41–68.
[22] J. Zhou, *Coord. Chem. Rev.* **2016**, *315*, 112–134.
[23] B. Krebs, *Angew. Chem. Int. Ed. Engl.* **1983**, *22*, 113–134.
[24] W. Schiwy, S. Pohl, B. Krebs, *Z. Anorg. Allg. Chem.* **1973**, *402*, 77–86.
[25] S. Santner, J. Heine, S. Dehnen, *Angew. Chem. Int. Ed.* **2016**, *55*, 876–893; *Angew. Chem.* **2016**, *128*, 886–904.
[26] A. Benkada, C. Näther, W. Bensch, *Z. Anorg. Allg. Chem.* **2020**, *646*, 1352–1358.
[27] F. Danker, T. Engesser, D. Broich, C. Näther, W. Bensch, *Dalton Trans.* **2021**, *50*, 18107–18117.
[28] R.-H. Duan, P.-F. Liu, H. Lin, S.-X. Huangfu, L.-M. Wu, *Dalton Trans.* **2017**, *46*, 14771–14778.
[29] W.-A. Li, J.-R. Li, B. Zhang, H.-Y. Sun, J.-C. Jin, X.-Y. Huang, M.-L. Feng, *ACS Appl. Mater. Interfaces* **2021**, *13*, 10191–10201.
[30] M.-L. Feng, D. Sarma, X.-H. Qi, K.-Z. Du, X.-Y. Huang, M. G. Kanatzidis, *J. Am. Chem. Soc.* **2016**, *138*, 12578–12585.
[31] Y. K. Kang, H. Lee, T. D. C. Ha, J. K. Won, H. Jo, K. M. Ok, S. Ahn, B. Kang, K. Ahn, Y. Oh, M.-G. Kim, *J. Mater. Chem. A* **2020**, *8*, 3468.
[32] A. C. Lokhande, P. T. Babar, V. C. Karade, M. G. Gang, V. C. Lokhande, C. D. Lokhande, J. H. Kim, *J. Mater. Chem. A* **2019**, *7*, 17118–17182.
[33] K. J. Norton, F. Alam, D. J. Lewis, *Appl. Sci.* **2021**, *11*, 2062.
[34] N. Pienack, A. Puls, C. Näther, W. Bensch, *Inorg. Chem.* **2008**, *47*, 9606–9611.
[35] A. Benkada, H. Reinsch, M. Poschmann, J. Krahmer, N. Pienack, W. Bensch, *Inorg. Chem.* **2019**, *58*, 2354–2362.
[36] C. L. Teske, H. Terraschke, S. Mangelsen, W. Bensch, *Z. Anorg. Allg. Chem.* **2020**, *646*, 1716–1721.
[37] Y. Shan, Y. Li, H. Pang, *Adv. Funct. Mater.* **2020**, *30*, 2001298.
[38] M. Duchardt, U. Ruschewitz, S. Adams, S. Dehnen, B. Roling, *Angew. Chem. Int. Ed.* **2018**, *57*, 1351–1355; *Angew. Chem.* **2018**, *130*, 1365–1369.
[39] Z. Zhang, E. Ramos, F. Lalère, A. Assoud, K. Kaup, P. Hartman, L. F. Nazar, *Energy Environ. Sci.* **2018**, *11*, 87–93.
[40] W. D. Richards, T. Tsujimura, L. J. Miara, Y. Wang, J. C. Kim, S. P. Ong, I. Uechi, N. Suzuki, G. Ceder, *Nat. Commun.* **2016**, *7*, 11009.
[41] E. P. Ramos, Z. Zhang, A. Assoud, K. Kaup, F. Lalère, L. F. Nazar, *Chem. Mater.* **2018**, *30*, 7413–7417.
[42] J. W. Heo, A. Banerjee, K. H. Park, Y. S. Jung, S.-T. Hong, *Adv. Energy Mater.* **2018**, *8*, 1702716.
[43] F. Hartmann, A. Benkada, S. Indris, M. Poschmann, H. Lühmann, P. Duchstein, D. Zahn, W. Bensch, *Angew. Chem. Int. Ed.* **2022**, *61*, e202202182.
[44] L. Gao, G. Bian, Y. Yang, B. Zhang, X. Wu, K. Wu, *New J. Chem.* **2021**, *45*, 12362–12366.
[45] T. Krauskopf, S. P. Culver, W. G. Zeier, *Inorg. Chem.* **2018**, *57*, 4739–4744.
[46] L. Zhang, D. Zhang, K. Yang, X. Yan, L. Wang, J. Mi, B. Xu, Y. Li, *Adv. Sci.* **2016**, *3*, 1600089.
[47] T. Kaib, S. Haddadpour, M. Kapitein, P. Bron, C. Schröder, H. Eckert, B. Roling, S. Dehnen, *Chem. Mater.* **2012**, *24*, 2211–2219.
[48] T. Kaib, P. Bron, S. Haddadpour, L. Mayrhofer, L. Pastewka, T. T. Järvi, M. Moseler, B. Roling, S. Dehnen, *Chem. Mater.* **2013**, *25*, 2961–2969.
[49] H. Wang, Y. Chen, Z. D. Hood, G. Sahu, A. S. Pandian, J. K. Keum, K. An, C. Liang, *Angew. Chem. Int. Ed.* **2016**, *55*, 8551–8555; *Angew. Chem.* **2016**, *128*, 8693–8697.
[50] A. Benkada, F. Hartmann, T. A. Engesser, S. Indris, T. Zinkevich, C. Näther, H. Lühmann, H. Reinsch, S. Adams, W. Bensch, *Chem. Eur. J.* **2023**, *29*, e202202318.
[51] F. Liebau, *Structural Chemistry of Silicates*, Springer, Berlin, Heidelberg, **1985**.
[52] R. D. Shannon, *Acta Crystallogr. Sect. A* **1976**, *32*, 751–767.
[53] C. Mundus, G. Taillades, A. Pradel, M. Ribes, *Solid State Nucl. Magn. Reson.* **1996**, *7*, 141–146.
[54] L. Protesescu, M. Nachtegaal, O. Voznyy, O. Borovinskaya, A. J. Rossini, L. Emsley, C. Copéret, D. Günther, E. H. Sargent, M. V. Kovalenko, *J. Am. Chem. Soc.* **2015**, *137*, 1862–1874.
[55] S. Hori, K. Suzuki, M. Hirayama, Y. Kato, R. Kanno, *Front. Energy Res.* **2016**, *4*, 38.
[56] J. T. S. Irvine, D. C. Sinclair, A. R. West, *Adv. Mater.* **1990**, *2*, 132–138.
[57] A. A. Coelho, Topas Academics 4.2. *Coelho Software: Brisbane*, **2007**.
[58] A. Altomare, M. Camalli, C. Cuocci, C. Giacovazzo, A. Moliterni, R. Rizzi, *J. Appl. Crystallogr.* **2009**, *42*, 1197–1202.
[59] Deposition Number CSD-2208659 ($Na_4Sn_2S_6$ (**II**)) contain the supplementary crystallographic data for this paper. These data are provided free of charge by the joint Cambridge Crystallographic Data Centre and Fachinformationszentrum Karlsruhe Access Structures service.
[60] N. J. Clayden, C. M. Dobson, A. Fern, *J. Chem. Soc. Dalton Trans.* **1989**, 843–847.

Manuscript received: November 7, 2022
Revised manuscript received: January 15, 2023
Accepted manuscript online: January 16, 2023